ACS OMEGA

Open Access

http://pubs.acs.org/journal/acsodf

Article

Lycium barbarum Polysaccharide-Stabilized Selenium Nanoparticles Deliver Triptolide to Induce Apoptosis for Pancreatic Cancer *In Vitro* and *In Vivo*

Xiaofang Li, Yunfang Su, Na Lin, Yujie Chen, Zhonghua Li, Zhenqiang Zhang,* Xuebin Zhao,* and Huahui Zeng*

Cite This: *ACS Omega* 2025, 10, 17108−17122

Read Online

ACCESS | Metrics & More | Article Recommendations | Supporting Information

ABSTRACT: Pancreatic cancer (PC), known as the "king of cancer," is a prevalent and aggressive form of malignant tumor affecting the digestive tract. Triptolide (TP), an epoxidized diterpenoid lactone extracted from *Tripterygium wilfordii*, shows promising antitumor activity. However, the systemic toxicity and poor water solubility of TP inhibit its clinical application. In this work, *Lycium barbarum* polysaccharide (LBP)-modified selenium nanoparticles (SeNPs), capable of reducing severe toxicity and enhancing solubility, have been designed, synthesized, and applied for the treatment of PC. *In vitro* release results revealed that TP showed an acid-dependent and sustained-release effect. In Pan02 cells, the IC50 values of TP and LBP-SeNPs@TP were 26.03 ± 2.82 ng/mL and 11.80 ± 2.64 ng/mL, respectively. Similarly, the IC50 values of TP and LBP-SeNPs@TP for L02 cells were 15.76 ± 0.58 ng/mL and 32.73 ± 2.61 ng/mL, suggesting enhanced antitumor efficacy along with reduced toxicity. Flow cytometry analysis demonstrated that LBP-SeNPs@TP exerted the most potent apoptotic effect, achieving an early apoptosis rate of 24.5% and a late apoptosis rate of 45.3%. Notably, the mitochondrial membrane potential was significantly reduced, while ROS production was increased in the LBP-SeNPs@TP group. LBP-SeNPs@TP could significantly inhibit tumor growth while minimizing toxicity. RT-qPCR analysis demonstrated that LBP-SeNPs@TP upregulated the mRNA expression of Bax, Cyt C, and Caspase-3, while downregulating Bcl-2 expression *in vitro* and *in vivo*. The immunohistochemical analysis of the tumor tissue further confirmed these results. Overall, LBP-SeNPs emerge as a promising platform for poorly soluble drugs, offering a potential therapeutic approach for pancreatic cancer.

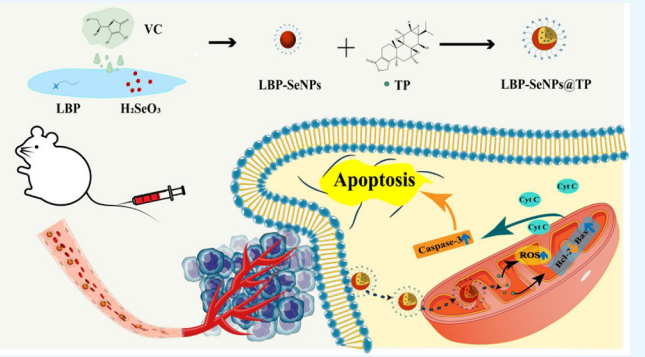

1. INTRODUCTION

Pancreatic cancer (PC) is a common digestive system tumor with the highest mortality rate.[1] Surgical resection is the most effective therapeutic method in clinical practice; however, the 5-year survival rate of PC is less than 5%. The lack of early diagnosis and high metastasis rate cause significant difficulties for surgical treatment, making the resection rate to be lower than 20%.[2] Chemotherapy remains the main treatment option for PC. The standard chemotherapy regimen is a combination of gemcitabine- and nanoalbumin-bound paclitaxel (Nab-paclitaxel), but patient survival is still extremely low, and serious side effects occur.[3] Therefore, reliable and effective treatments are still urgently needed.

Triptolide (TP), an active epoxidized diterpenoid lactone extracted from *Tripterygium wilfordii*, has potent antitumor, anti-inflammatory, and immunosuppressive properties.[4] TP inhibits cancer cell growth and exhibits excellent broad-spectrum activity against a variety of cancers.[5] A water-soluble prodrug of triptolide, minnelide, is currently being used in phase II clinical trials for advanced pancreatic cancer.[6] Extensive investigation into the mechanism of TP in the treatment of PC reveals its ability to promote apoptosis activity,[5] primarily through the death receptor-mediated apoptosis pathway and mitochondrial-dependent apoptosis pathway.[7]

However, the poor water solubility and severe toxicity of TP limit its application. Various TP platforms, such as solid lipid nanoparticles,[8] liposomes,[9,10] polymer micelles,[11,12] nano-emulsions,[13] and inorganic nanocarriers[14−16] have been developed to improve solubility and reduce toxicity. Among inorganic carriers, selenium nanoparticles (SeNPs), with good bioavailability, *in vivo* degradation, easy synthesis, and low

Received: May 19, 2024
Revised: April 6, 2025
Accepted: April 14, 2025
Published: April 22, 2025

toxicity, have not yet been used for loading TP.[17] SeNPs are prone to aggregation in aqueous solutions due to their high surface energy.[18] Therefore, SeNPs are often modified with macromolecular stabilizers. As biological stabilizers, polysaccharides (PS) possess complex branched structures and active hydroxyl groups, which can serve as soft templates to control the size of SeNPs.[19] Among these, traditional Chinese medicine polysaccharides are excellent candidates for stabilizing SeNPs due to their low toxicity, structural diversity, and good biocompatibility.[20]

In this study, SeNPs with traditional Chinese medicine polysaccharides as stabilizers were prepared, displaying high bioavailability and good safety. The obtained SeNPs loaded TP to form a stable nanodrug. The detoxification effect, enhanced anti-pancreatic cancer effect, and preliminary antitumor mechanisms of the nanodrug *in vivo* and *in vitro* were further explored, paving the way for the future application of SeNPs@TP in the treatment of PC.

2. MATERIALS AND METHODS

2.1. Materials. *Ganoderma lucidum* polysaccharides (GLP), *astragalus* polysaccharides (AP), *brown algae* polysaccharides (BAP), and *Lycium barbarum* polysaccharides (LBP) were purchased from Xi'an Baichuan Biotechnology Co., Ltd. (Shanxi, China). Selenite and ascorbic acid were obtained from Kermel Chemical Reagent Co. Ltd. (Tianjin, China). A 3.5 kDa dialysis bag, PBS, penicillin streptomycin mixture, DMEM, Reactive Oxygen Species Assay Kit with DCFH-DA, Mitochondrial Membrane Potential Assay Kit with JC-1, 4% paraformaldehyde, BCA Protein Assay Kit, and Trizol were obtained from Solarbio Technology Co., Ltd. (Beijing, China). Fetal bovine serum (FBS) was purchased from Biological Industries (Shanghai, China). Methanol (CP) was purchased from Tianjin Fuyu Fine Chemical Co., Ltd. (Tianjin, China). Methanol (LC) and acetonitrile (LC) were purchased from Honeywell Burdick & Jackson (USA). Cell freezing medium was obtained from Suzhou Xinsaimei Biotechnology Co., Ltd. (Jiangsu, China). CCK-8, Annexin V-FITC/PI Cell Apoptosis Detection Kit, and crystal violet (high-purity biological dyeing grade) were obtained from MeilunBio (Liaoning, China). Isopropanol was purchased from Damao Chemical Reagent Factory (Tianjin, China). The First Strand cDNA Synthesis Kit was sourced from Beyotime (Shanghai, China). dNTP Mix was obtained from Thermo Fisher Scientific (Waltham, MA, USA). DEPC water was purchased from Hefei White Shark Biotechnology Co., Ltd. (Anhui, China). Kits for the analysis of blood urea nitrogen (BUN), creatinine (Crea), serum alanine aminotransferase (ALT), and aspartate aminotransferase (AST)) were obtained from Nanjing Jiancheng Bioengineering Institute (Jiangsu, China). Anti-Ki67 Mouse mAb, secondary antibody HRP-labeled goat-antirabbit IgG, 3% H_2O_2, BSA, hematoxylin stain solution, HE stain solution, hematoxylin differentiation solution, hematoxylin blue returning solution, and DAB chromogenic agent were all purchased from Wuhan Servicebio Technology Co., Ltd. Ethanol, xylene, and neutral balsam were purchased from Sinopharm Chemical Reagent Co., Ltd. Distilled and deionized (DI) water was used in all experiments.

Mouse pancreatic cancer cells (Pan02) and liver cells (L02) were purchased from the American Type Culture Collection. Eight-week-old SPF-grade C57BL/6J mice, weighing 18−20 g, were purchased from Jinan Pengyue Experimental Animal Breeding Co., Ltd. with production license number 20190003 and raised at the Animal Experimental Center of Henan University of Chinese Medicine. The mice were adaptively fed in an environmental control area (25 ± 1 °C, 12-h light and dark cycle) for 7 days and provided with water and food. This study was approved by the Animal Ethics Committee of Henan University of Chinese Medicine (No. DWLL202110005).

2.2. Synthesis of PS-SeNPs and LBP-SeNPs@TP. Before the experiment, 225 mg of *Ganoderma lucidum* polysaccharides, *Astragalus polysaccharides*, *Brown algae* polysaccharides, or *Lycium barbarum* polysaccharides were completely dissolved in 240 mL of deionized water to form polysaccharide (PS) solutions. Selenite solution was freshly prepared by dissolving 232 mg of selenite completely in 120 mL of deionized water. The obtained solution was mixed thoroughly with the above PS solution and stirred overnight at room temperature. A total of 1585 mg of ascorbic acid was completely dissolved in 90 mL of deionized water and added dropwise to the mixture above. After reacting at room temperature for 30 min, the obtained solution was dialyzed at 4 °C for 72 h using a dialysis bag (MWCO: 3.5 kDa). Finally, the solution was freeze-dried to obtain the LBP-SeNPs. As mentioned above, LBP-SeNPs with final concentrations of 0.5, 1, 2, and 4 mg/mL (denoted as $^{0.5}$LBP-SeNPs, $^{1.0}$LBP-SeNPs, $^{2.0}$LBP-SeNPs, and $^{4.0}$LBP-SeNPs, respectively) were synthesized.

An appropriate amount of TP (the molar ratio of Se input in LBP-SeNPs and TP was 3:1, 5:1, 10:1, and 20:1, respectively) was completely dissolved in a small amount of methanol. The obtained LBP-SeNPs aqueous solution was evenly mixed with the methanol solution of TP, stirred at room temperature for 8 h, and then dialyzed at 4 °C using a dialysis bag (MW: 3.5 kDa). Finally, the solution was lyophilized to obtain LBP-SeNPs@TP.

2.3. Characterizations of LBP-SeNPs and LBP-SeNPs@TP. Appropriate concentrations of LBP-SeNPs and LBP-SeNPs@TP aqueous solutions were prepared. Deionized water was used as the blank control group for baseline calibration. Subsequently, UV−vis spectral scanning was performed on the samples within the range of 190−800 nm using a UV−vis spectrophotometer (Thermo Scientific Evolution 201). Fourier transform infrared (FT-IR) spectrum samples were recorded on an Equinox 55 IR spectrometer with a scanning range of 500−4000 cm^{-1}. A drop of the LBP-SeNPs or LBP-SeNPs@TP sample was placed onto a copper mesh coated with a carbon film, dried at room temperature, and then negatively stained with a 2% (w/v) phosphotungstic acid solution. After drying, the morphology and size were observed using a transmission electron microscope (JEOL, JEM-1400). The hydrodynamic diameter and Zeta potential were obtained using a Zetasizer Nano ZS (Brookhaven NanoBrook 90Plus PALS). The stability was also measured using a particle size analyzer. A 1 mg/mL aqueous solution of LBP-SeNPs or LBP-SeNPs@TP was prepared, stored at 4 °C, and sampled weekly to measure changes in particle size using the Zetasizer Nano ZS. In addition, the samples were dissolved in DMEM, FBS, PBS, or DMEM + 10% FBS and stored at 37 °C in a constant temperature shaker set at 100 rpm for 24 h. The particle size changes were detected at 0, 2, 4, 6, 8, 10, 12, and 24 h to evaluate stability *in vitro*.

The water solubility of TP in LBP-SeNPs@TP was measured using a UV−vis spectrophotometer (Thermo Scientific Evolution 201). Thirty milligrams of LBP-SeNPs@TP was added to 1 mL of deionized water. The obtained solution was shaken evenly, sonicated for 15 min, vortexed for

https://doi.org/10.1021/acsomega.4c04743
ACS Omega 2025, 10, 17108−17122

3 min, and centrifuged at 12000 rpm for 10 min. The supernatant was diluted 100 times and analyzed using a UV−vis spectrophotometer at a wavelength of 218 nm, with deionized water serving as the blank group.

The loading efficiency was determined using HPLC (LC-2030C 30 Plus) equipped with a Shim-pack GIST C18 chromatographic column (4.6 × 250 mm, 5 μm) and a UV−vis photodiode array detector. The HPLC analysis conditions were as follows: mobile phase, acetonitrile:water = 33:67 at 1 mL/min; detection wavelength, 218 nm; and column temperature, 40 °C.

The drug encapsulation efficiency and drug loading of TP were calculated using the following formulas:

Encapsulation efficiency (EE%) = (weight of loaded TP/weight of TP in feed) × 100%

Drug loading (DL%) = (weight of loaded TP/weight of LBP-SeNPs@TP) × 100%

2.4. *In Vitro* Drug Release of LBP-SeNPs@TP. *In vitro* drug release of LBP-SeNPs@TP was measured using the dialysis bag (MWCO: 3.5 kDa, Solarbio) method. First, the release medium was prepared by mixing phosphate-buffered saline (PBS) solution with 0.5 vol% Tween at pH 7.4 and 5.0. Then, the dialysis bag containing 2 mL of TP solution was placed in 40 mL of release medium at pH 7.4. Additionally, 2 mL of LBP-SeNPs@TP solution was prepared at pH 7.4 or 5.0 and stirred at a speed of 100 r/min at 37 °C. Subsequently, 1 mL of release medium was taken out at 0.5, 1, 2, 3, 4, 5, 6, 8, 10, 12, 24, 36, 48, and 72 h, respectively, and supplemented with the same amount of fresh medium. The released TP was detected using HPLC, the cumulative release amount and cumulative release percentage were calculated, and the drug release curve was drawn.

2.5. *In Vitro* Cytotoxicity Study by Using CCK-8 Assay. This study used the Cell Proliferation and Toxicity Detection Kit (CCK-8) to detect the cytotoxicity of TP and LBP-SeNPs@TP on L02 and Pan02 cells. Cells were cultured in a 96-well plate at 37 °C with 1% penicillin−streptomycin double-antibody solution, 10% FBS, and 89% DMEM complete medium. For L02 cells, free TP and LBP-SeNPs@TP containing TP concentrations of 4, 8, 16, 24, 32, 40, 48, 56, and 64 ng/mL were used to evaluate cytotoxicity. For Pan02 cells, free TP and LBP-SeNPs@TP with TP concentrations of 8, 16, 24, 32, 40, and 48 ng/mL were investigated. After treatment for 48 h, 10 μL of CCK-8 was added to each well and incubated for 0.5−2 h. The absorbance of the solution was measured at 450 nm using a microplate reader (Thermo Fisher, 1510), and cell viability was calculated using the formula: Cell viability = (administration group − blank group)/(control group − blank group) × 100%. The drug concentration (IC_{50}) at 50% inhibition was determined using GraphPad Prism 8.0.1 software.

2.6. Apoptosis Detection by Annexin V-FITC/PI Double Stain. Pan02 cells were cocultured with complete medium (control group), free TP (10 ng/mL), LBP-SeNPs, TP/LBP-SeNPs Mix (TP: 10 ng/mL), or LBP-SeNPs@TP (TP: 10 ng/mL) for 48 h, collected, and rinsed. The control group cells were divided into two parts. One part of the cells was resuspended in 500 μL of Apoptosis Positive Control Solution and placed on ice for 30 min. After centrifugation at 3000 rpm for 5 min, the supernatant was discarded, and 1 mL of 1 × binding buffer was added. The other part of the cells was resuspended in 500 μL of 1 × binding buffer and mixed with the first portion to form 1.5 mL of cell suspension. The 1.5 mL of cell suspension was divided into three equal parts, namely, the PI group, FITC group, and control group. Ten microliters of PI reagent was added to the PI group, 5 μL of FITC reagent was added to the FITC group, and 10 μL of PI reagent and 5 μL of FITC reagent were added to the control group. All groups were incubated at room temperature in the dark for 15 min. For every administration group, 100 μL of 1 × binding buffer, 10 μL of PI reagent, and 5 μL of FITC reagent were added and incubated at room temperature in the dark for 15 min. The cells were tested using flow cytometry (BD FACSCanto II Flow Cytometer).

2.7. Mitochondrial Membrane Potential Measurement by JC-1. The working solution was prepared as follows: ① JC-1 staining working solution: 50 μL of 200 × JC-1 was mixed with 8 mL of ultrapure water, and 2 mL of 5 × buffer solution was added to obtain the JC-1 staining working solution. ② JC-1 staining buffer: 1 mL of 5 × JC-1 staining buffer and 4 mL of distilled water were mixed thoroughly to obtain 1 × JC-1 staining buffer, which was then placed in an ice bath.

Pan02 cells were treated as described in Section 2.6, and 1 mL of JC-1 staining solution was added. The cells were incubated in the incubator for 20 min, rinsed with 1 × JC-1 staining buffer, and observed using a fluorescence microscope (Nikon Ti2-U).

Fluorescence intensity was quantified using ImageJ software, and the specific process was as follows: the image was opened, converted into a grayscale image, adjusted to the appropriate threshold and parameters, and clicked *Measure* to obtain the analysis results. Finally, the data were exported, and GraphPad Prism 8.0.1 software was used for subsequent analysis and plotting.

2.8. Determination of ROS Generation by DCFH-DA. The working solution was prepared as follows. DCFH-DA (10 mM) was diluted with serum-free culture medium to obtain 10 μmol/L DCFH-DA. Pan02 cells were treated, as shown in Section 2.6 and 1 mL of DCFH-DA (10 μmol/L) was added. The cells were incubated in the incubator for 20 min and rinsed with serum-free culture medium to thoroughly remove the extra DCFH-DA that had not entered the cells. Finally, fluorescence was evaluated using a fluorescence microscope (Nikon, Ti2-U). The quantitative process is described in Section 2.7.

2.9. mRNA Expression Analysis by RT-qPCR. Trizol was added to Pan02 cells or tumor tissues to extract RNA, and the concentration and purity of RNA were confirmed using an ultramicro spectrophotometer (Thermo NanoDrop 2000). RNA was reverse-transcribed by using a BeyoRT III First Strand cDNA Synthesis Kit with gDNA EZeraser. RT-qPCR was then conducted using a real-time fluorescent quantitative PCR system (Thermo Fisher, 5020). The DNA primers used were as follows: *Bax* (GCCTTTTTGCTACAGGGTTTCAT, TATTGCTGTCCAGTTCATCTCCA), *Bcl-2* (AGGATTGTGGCCTTCTTTGAGT, ACAGCCAGGAGAAATCAAACAGA), *Caspase3* (TGGAATGTCATCTCGCTCTGGT, GAAGAGTTTCGGCTTTCCAGTC), *Cyt-C* (CCAACAAGAACAAAGGCATCAC, CTGCCCTTTCTCCCTTCTTCTTA), and *GAPDH* (CCTCGTCCCGTAGACAAAATG, TGAGGTCAATGAAGGGGTCGT).

2.10. Establishment of Pancreatic Cancer Mouse Model and Administration. Pan02 cells were collected and resuspended in PBS to a concentration of 5 × 1 × 10^6

https://doi.org/10.1021/acsomega.4c04743
ACS Omega 2025, 10, 17108−17122

cells/mL. Fifty microliters of Pan02 cells were injected into the subcutaneous area of the right abdomen of C57BL/6J mice. When the tumor nodule reached approximately 100 mm^3, the modeling was completed. Mice were randomly divided into six groups (n = 5): model group, LBP-SeNPs group, TP group (0.2 mg/kg), TP/LBP-SeNPs mix group (containing TP: 0.2 mg/kg), and LBP-SeNPs@TP groups (containing TP: 0.2 and 0.4 mg/kg, respectively). Mice were injected through the tail vein and administered treatments every 2 days for 2 weeks. At the same time, a vernier caliper was used to record the tumor volume of the mice every 2 days using the formula V (mm^3) = length (mm) × width^2 (mm^2)/2. After treatment, the mice were sacrificed to collect the serum, heart, liver, kidneys, testicles, and tumor tissues from each group.

2.11. *In Vivo* Safety Evaluation. *2.11.1. Changes of Weight, Liver, and Kidney Function.* The weight of the mice in each group was measured on the day before administration and every 2 days after administration. After administration, blood samples were taken from the mouse eyeballs and centrifuged at 4 °C at 4000 rpm for 15 min. The supernatant was then stored in a refrigerator at −80 °C. Alanine transaminase (ALT), aspartate transaminase (AST), blood urea nitrogen (BUN), and creatinine (CR) kits were used to evaluate the hepatorenal toxicity of each drug in mice according to the instructions.

2.11.2. Histological Staining. The mice were sacrificed, and the organs (heart, liver, kidney, testicles, and tumor) from each group were quickly fixed with 4% formalin at 4 °C. After embedding sections, tissue dewaxing, hydration, hematoxylin-eosin staining, dehydration, and film sealing, the histological changes were observed using a digital pathological section scanning system (KF-PRO-005).

Heart, liver, kidney, testicles, and tumor tissues of each group were stored in 4% paraformaldehyde, and the corresponding paraffin sections were prepared. After dewaxing and hydration, the sections were soaked twice in xylene for 5 min each time and then soaked in anhydrous ethanol, 95% ethanol, 85% ethanol, and 70% ethanol in sequence for 5 min each and rinsed with PBS. The processed sections were stained in hematoxylin staining solution for 10 min, differentiated with 1% hydrochloric acid differentiation solution for 2−5 min, and reversed blue with 0.1 M PBS for 10 min. The histological changes were observed using a digital pathological section scanning system (KF-PRO-005).

2.12. Immunohistochemical (IHC) Analysis. Five micrometer tumor tissue sections were prepared to detect the expression of Ki67. After dehydration of the paraffin sections, they were placed in an EDTA (pH 9.0) antigen repair solution and transferred to a microwave oven for antigen repair. Then, the sections were placed in 3% H_2O_2 solution and incubated in the dark for 25 min to block endogenous peroxidase, followed by sealing at room temperature with 3% BSA for 30 min. Subsequently, the slices were removed from the sealing solution and incubated with the primary antibody anti-Ki67 (1:200) at 4 °C overnight, and the fluorescent secondary antibody, HRP-labeled goat anti-rabbit, was incubated at room temperature for 50 min. Finally, DAB staining, hematoxylin staining of the cell nucleus, and dehydration sealing were conducted in sequence. The average optical density was analyzed using ImageJ 1.4.3.67 software after observing and capturing images under the pathological section scanner (3D HISTECH Pannoramic MIDI).

2.13. Statistical Analysis. All data were statistically analyzed using GraphPad Prism 8.0.1 software and expressed as mean ± SD. Statistical differences were determined by one-way analysis of variance (ANOVA) with post hoc tests or by the Student's t test.

3. RESULTS

3.1. Preparation and Characterization of PS-SeNPs. Orange-red SeNPs were prepared by an oxidation−reduction reaction using ascorbic acid to reduce the level of Se^{4+} in selenite. Considering that SeNPs are extremely unstable and prone to aggregation and precipitation into black elemental selenium (Figure S1), polysaccharide biomolecules, such as mushroom polysaccharides,[21] *Rosa roxburghii* fruit polysaccharide,[22] *Polyporus umbellatus* polysaccharide,[23] etc., have been used to modify SeNPs to alter their aggregation propensity. This study selected common traditional Chinese medicine polysaccharides, including *Ganoderma lucidum* polysaccharides (GLP), *Astragalus* polysaccharides (AP), *Brown algae* polysaccharides (BAP), and *Lycium barbarum* polysaccharides (LBP) as modifiers to stabilize SeNPs. As shown in Figure 1,

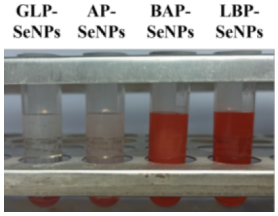

Figure 1. Photographs of the SeNP aqueous solution modified with *Ganoderma lucidum* polysaccharides, *Astragalus* polysaccharides, *Brown* algae polysaccharides, and *Lycium barbarum* polysaccharides, respectively.

GLP-SeNP and AP-SeNP aqueous solutions precipitated rapidly after reduction, and the BAP-SeNP solution showed significant turbidity, indicating their poor stability and nonuniform morphology of SeNPs. Notably, LBP-SeNPs presented a uniform and transparent orange-red solution, indicating that they could stabilize SeNPs and were good modifiers.

The formation of LBP-SeNPs is illustrated in Figure 2A. Different concentrations of LBP were used to stabilize SeNPs, as shown in Figure 2B, presenting a clear and transparent orange-red solution. The UV−vis spectra recorded that the characteristic absorption peak of SeNPs appeared at 256 nm for $^{0.5}$LBP-SeNPs, $^{1.0}$LBP-SeNPs, $^{2.0}$LBP-SeNPs, and $^{4.0}$LBP-SeNPs, implying the successful formation of LBP-SeNPs. Zeta potential, particle size distribution, and stability for different concentrations of LBP-modified SeNPs were measured to investigate the optimal LBP concentration (Figure 2D−G). When the LBP concentration was 0.5 mg/mL, the absolute value of the Zeta potential for $^{0.5}$LBP-SeNPs was at its minimum. There was no significant difference observed among the other three groups (Figure 2D). The diameters of $^{0.5}$LBP-SeNPs were around 80 nm, while the diameters of the other groups were around 60 nm (Figure 2E). During the 42-day stability assessment of size and PDI, only the size of $^{0.5}$LBP-SeNPs displayed slight enhancement, implying poor stability for $^{0.5}$LBP-SeNPs and good stability for the other groups (Figure 2F,G). Therefore, $^{1.0}$LBP-SeNPs were selected as the optimal carrier with an average size of 66.32 ± 0.26 nm. In the

https://doi.org/10.1021/acsomega.4c04743
ACS Omega 2025, 10, 17108−17122

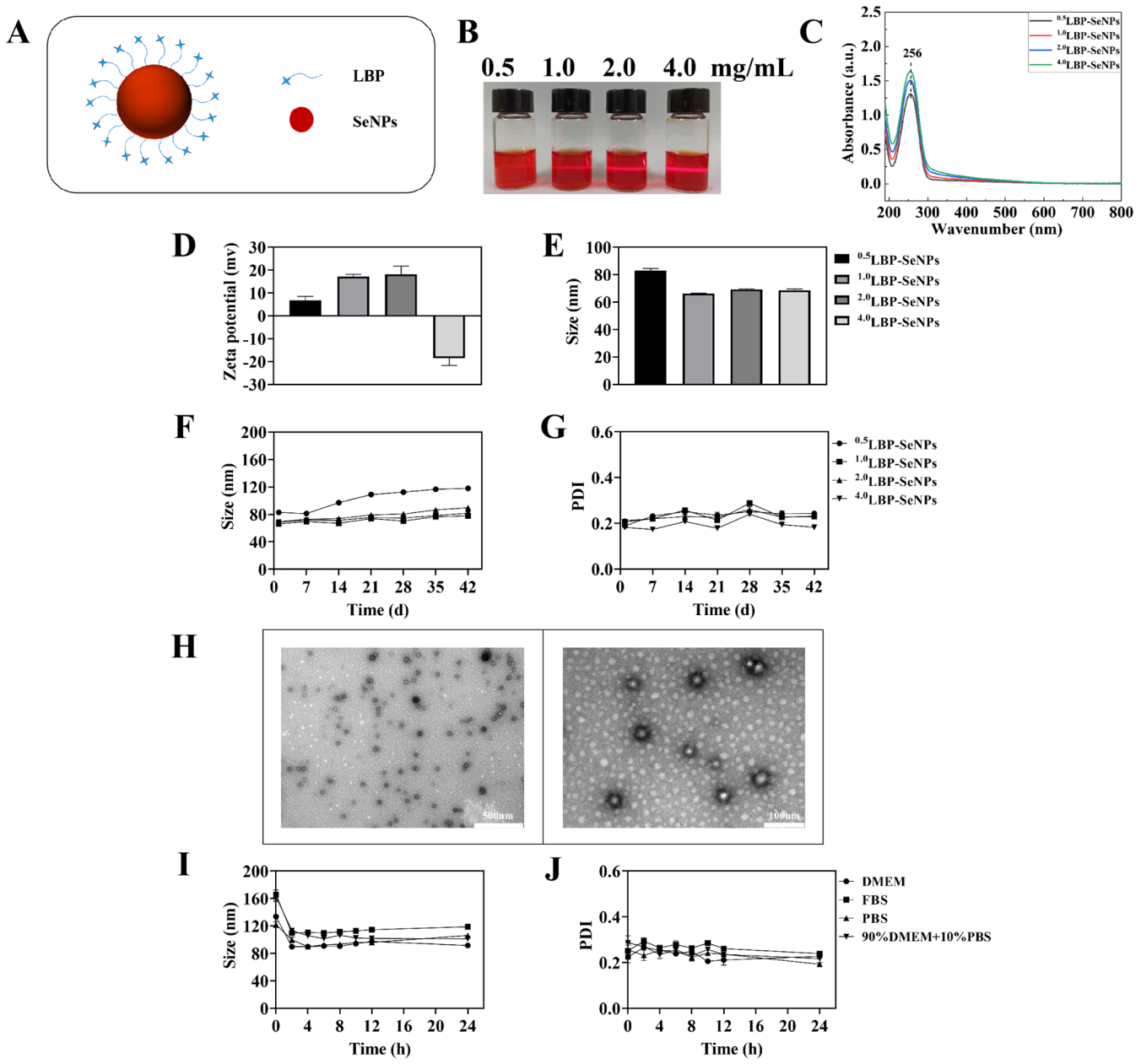

Figure 2. Structural and property characterization of LBP-SeNPs. (A) Proposed illustration, (B) photographs, (C) UV−vis spectra, (D) Zeta potential, (E) particle size, (F) size and (G) PDI change in aqueous solution, (H) TEM image (scale bar, 500 and 100 nm), and (I) size and (J) PDI change of $^{1.0}$LBP-SeNPs in different media.

following text, all references to LBP-SeNPs refer to $^{1.0}$LBP-SeNPs.

As shown in Figure 2H observed from the TEM image, the morphology presented regular spherical nanoparticles with size ranges of 25−35 nm. In order to investigate the *in vivo* stability of LBP-SeNPs, the particle size and PDI changes of LBP-SeNPs dispersed in DMEM, FBS, PBS, and DMEM + 10% FBS at 37 °C were monitored. LBP-SeNPs showed no significant changes within 24 h (Figure 2I,J), indicating that they could remain stable in various biological media.

3.2. Preparation and Characterization of LBP-SeNPs@TP. LBP-SeNPs@TP were prepared by loading TP onto the surfaces of LBP-SeNPs, and the structural schematic diagram is shown in Figure 3A. TEM photographs (Figure 3B) showed that LBP-SeNPs@TP was a spherical and uniformly monodisperse nanosphere with a particle size of 40−60 nm. TP exhibited C═O stretching vibration peaks at 1769 cm^{-1} in the FT-IR spectra (Figure 3C). For LBP-SeNPs@TP, the peak also appeared, and the C═O peak was shifted to 1772 cm^{-1}, indicating that TP was successfully loaded onto LBP-SeNPs. The UV−vis spectra (Figure 3D) showed that the characteristic peak of TP appeared at 206 nm, and LBP-SeNPs had an absorption peak at 264 nm, which was the characteristic peak of SeNPs. The absorption peak of TP shifted from 206 to 222 nm in LBP-SeNPs@TP, which may be due to the interaction between functional groups such as C═O and O−H of TP with Se nanoparticles. The UV−vis spectra confirmed that TP was successfully loaded onto the LBP-SeNPs. A significant peak appeared at 12.5 min in the HPLC spectra (Figure 3E) for both standard TP and LBP-SeNPs@TP, further indicating that the prepared LBP-SeNPs@TP contained TP. LBP-SeNPs@TP were uniform nanospheres with a 19.27 ± 1.01 mV potential

https://doi.org/10.1021/acsomega.4c04743
ACS Omega 2025, 10, 17108−17122

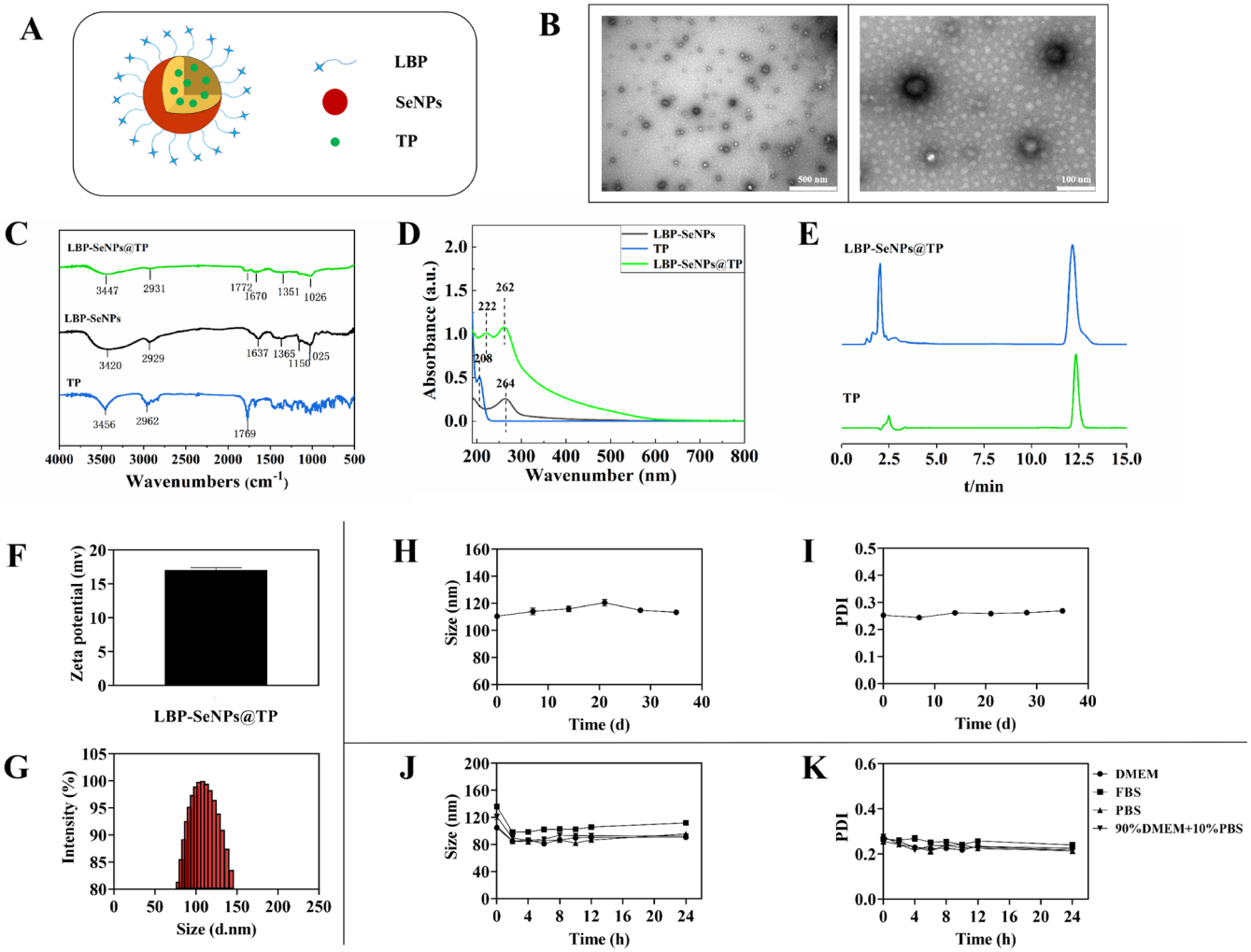

Figure 3. Structural and Physical Characterization of LBP-SeNPs@TP. (A) Proposed illustration, (B) TEM image (scale bar, 500 and 100 nm), (C) FT-IR spectra, (D) UV−vis spectra, (E) HPLC spectra of standard TP and LBP-SeNPs@TP, (F) Zeta potential. Stability characterization. (G) Particle size distribution, (H) size and (I) PDI change in an aqueous solution, and (J) size and (K) PDI change of LBP-SeNPs@TP in different media.

Table 1. Effect of the Input Molar Ratio of Se and TP on LBP-SeNPs@TP[a]

Input molar ratio of Se and TP	Encapsulation efficiency/%	Drug loading/%	Particle size/(nm)	PDI	Zeta potential (mV)
5:1	14.90 ± 0.45%	5.56 ± 0.20%	113.8 ± 3.44	0.24 ± 0.02	17.03 ± 0.85
10:1	18.40 ± 0.44%	3.46 ± 0.20%	115.96 ± 4.61	0.24 ± 0.02	19.27 ± 1.01
20:1	26.06 ± 0.28%	2.36 ± 0.13%	108.57 ± 2.69	0.24 ± 0.02	19.57 ± 2.63

[a]Values expressed are mean ± SD, n = 3.

and an average particle size of 113.8 ± 3.44 nm (Figure 3F,G). The obtained particle size was larger than that measured by TEM as DLS analysis focused on the hydrodynamic diameter of the nanospheres, and LBP-SeNPs@TP were surrounded by H_2O.[24]

To investigate the stability of LBP-SeNPs@TP, the particle size and PDI variation were observed in an aqueous solution maintained at 4 °C for a duration of 35 days (Figure 3 H−I). Additionally, monitoring was conducted in DMEM, FBS, PBS, and DMEM + 10% FBS at 37 °C for 24 h (Figure 3 J−K). There was no significant change in either particle size or PDI, suggesting that LBP-SeNPs@TP could be stored stably for 35 days at 4 °C. Similarly, there was no significant change in either particle size or PDI within 24 h in DMEM, FBS, PBS, or DMEM + 10% FBS at 37 °C, indicating that it could stably exist in a simulated *in vivo* environment.

TP exhibits poor water solubility, with a solubility of only 17 μg/mL in water.[25] LBP-SeNPs@TP were developed to enhance the water solubility of TP. A UV−vis spectrophotometer was used to measure water solubility (standard curve of TP by UV−vis spectra, Figure S2). LBP-SeNPs@TP, an orange-red solid, exhibited more than a 4-fold greater water solubility (1253.43 ± 3.69 μg/mL) compared to TP (17 μg/mL). These findings demonstrated a significant improvement in the water solubility of LBP-SeNPs@TP compared to free TP.

According to the method described in Section 2.2, LBP-SeNPs@TP were prepared by varying the molar ratios of Se to TP, specifically 3:1, 5:1, 10:1, and 20:1. When the Se:TP ratio

https://doi.org/10.1021/acsomega.4c04743
ACS Omega 2025, 10, 17108−17122

was 3:1, the resulting particle size (440.19 ± 41.03 nm) and PDI (0.339 ± 0.011) did not meet the experimental requirements. Table 1 summarizes the encapsulation efficiency, drug loading, particle size, PDI, and Zeta potential. The standard curve of TP obtained via HPLC spectra is displayed in Figure S3. Analysis of the results revealed that there was no significant difference in particle size and Zeta potential among the three feeding ratios of LBP-SeNPs@TP. Considering the drug loading, an Se:TP ratio of 5:1 was determined to be the optimal feeding ratio, achieving a drug loading of 5.56 ± 0.20% and an encapsulation efficiency of 14.90 ± 0.45% for TP.

3.3. *In Vitro* Drug Release from LBP-SeNPs@TP. The release of TP from LBP-SeNPs@TP was assayed by using the dialysis bag method. Given the slightly acidic nature of the tumor microenvironment, the acid-dependent release behavior was a crucial aspect in designing the cancer drug delivery system. The simulated release of TP in the normal physiological environment (pH 7.4) and the tumor cell microenvironment (pH 5.0) was conducted. The TP content collected at various time intervals was quantified by HPLC to calculate the cumulative release percentage of TP *in vitro* within 72 h. Figure 4 shows that TP exhibits a rapid release

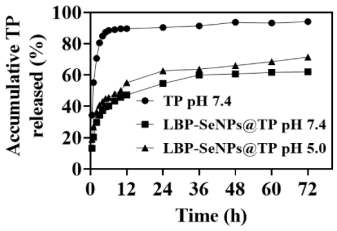

Figure 4. *In vitro* release of TP and LBP-SeNPs@TP in different environments (pH 7.4 and 5.0).

trend at pH 7.4, achieving a cumulative release of approximately 80% within 3 h. Under the same pH conditions, the release content of TP from LBP-SeNPs@TP only reaches about 62% at 72 h, indicating the significant sustained release effect of the prepared drug system. At pH 5.0, the overall release trend of TP from LBP-SeNPs@TP is comparable to that at pH 7.4, but with a faster TP release rate, reaching around 71% at 72 h. This suggested that the release rate of TP in LBP-SeNPs was associated with an acidic environment, which may be attributed to the hydrogen bonding interaction between LBP and SeNPs. At pH 7.4, the strong hydrogen bonding between SeNPs and LBP enhanced its stability and hindered the release of TP. However, at pH 5.0, the hydrogen bonding was weakened or disrupted, facilitating the release of TP from LBP-SeNPs@TP.[26,27] The above results demonstrated that LBP-SeNPs exhibited both sustained release and acid-dependent effects, making it advantageous for the controlled release of cancer drugs.

3.4. *In Vitro* Cytotoxicity of LBP-SeNPs@TP. The CCK-8 experiment was used to detect the *in vitro* cytotoxicity of TP, LBP-SeNPs, and LBP-SeNPs@TP against pancreatic cancer (Pan02) cells and normal liver (L02) cells. As shown in Figure 5A, the IC_{50} of TP and LBP-SeNPs@TP were 26.03 ± 2.82 and 11.80 ± 2.64 ng/mL, respectively, in Pan02 cells. Conversely, in L02 cells, the IC_{50} values of TP and LBP-SeNPs@TP were 15.76 ± 0.58 and 32.73 ± 2.61 ng/mL, respectively (Figure 5B). The above results demonstrated a significant increase in anticancer activity, exceeding a 2-fold

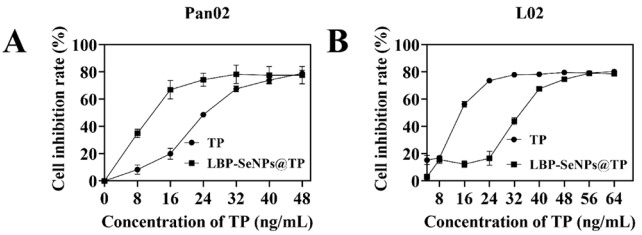

Figure 5. (A) *In vitro* cytotoxicity of TP and LBP-SeNPs@TP to Pan02 cells. (B) *In vitro* cytotoxicity of TP and LBP-SeNPs@TP to L02 cells (mean ± SD, n = 3).

enhancement, upon loading TP onto LBP-SeNPs. This enhancement was likely attributed to the improved cellular uptake of TP by cancer cells when delivered via LBP-SeNPs@TP.[17] Furthermore, the toxicity toward normal cells was reduced by approximately 2-fold, potentially due to the sustained release effect of TP from LBP-SeNPs@TP. Notably, at 48 and 56 ng/mL of TP in Pan02 and L02 cells, respectively, the cell inhibition rates of TP and LBP-SeNPs@TP were comparable, indicating a near-complete release of TP from LBP-SeNPs@TP. Compared to free TP, LBP-SeNPs@TP exhibited a stronger inhibitory effect on the growth of mouse pancreatic cancer cells, indicating that LBP-SeNPs could effectively enhance the anticancer efficiency of TP. Additionally, LBP-SeNPs@TP could decrease the toxicity of TP to normal cells, highlighting the advantages of high efficiency and low toxicity.

3.5. LBP-SeNPs@TP-Induced Apoptosis Analysis. Flow cytometry was utilized to evaluate the induced apoptosis effect of TP, LBP-SeNPs, TP/LBP-SeNPs Mix, and LBP-SeNPs@TP in Pan02 cells. As shown in Figure 6, the LBP-SeNP group exhibited an early apoptosis rate of 3.02% and a late apoptosis rate of 7.10%, suggesting that the carrier possessed inherent apoptotic activity. At the same TP concentration, the early apoptosis rate increased progressively from 7.28% in the free TP group to 14.2% in the TP/LBP-SeNPs Mix and ultimately to 24.0% in the LBP-SeNPs@TP group. Similarly, the late apoptosis rate rose from 10.7% in the free TP group to 12.9% in the TP/LBP-SeNPs Mix group, reaching 45.3% in the LBP-SeNPs@TP group. Notably, the TP/LBP-SeNPs Mix group displayed a slight elevation in the total apoptosis rate compared with the TP group ($p < 0.01$), but these rates were significantly lower than those in the LBP-SeNP @TP group ($p < 0.001$, $p < 0.0001$). The above findings demonstrated that the carrier LBP-SeNPs could effectively enhance TP-induced apoptosis in Pan02 cells.

3.6. LBP-Senps@TP-Induced Mitochondrial Membrane Potential (MMP) Disruption. The decrease in the mitochondrial membrane potential (MMP) serves as an indicator of early apoptosis. To explore the effect of drugs on MMP after entering the mitochondria, the fluorescence probe JC-1 was used to detect changes in MMP following treatment with LBP-SeNPs, TP, TP/LBP-SeNPs Mix, and LBP-SeNPs@TP. The underlying principle is that when the MMP is high, JC-1 accumulates within the mitochondrial matrix, forming polymers that produce red fluorescence. Conversely, when the MMP is low, JC-1 fails to aggregate in the mitochondrial matrix, resulting in green fluorescence. Therefore, the alteration in MMP can be assessed by the ratio of green-to-red fluorescence. As illustrated in Figure 7, there was no significant change in the ratio of green-to-red

https://doi.org/10.1021/acsomega.4c04743
ACS Omega 2025, 10, 17108−17122

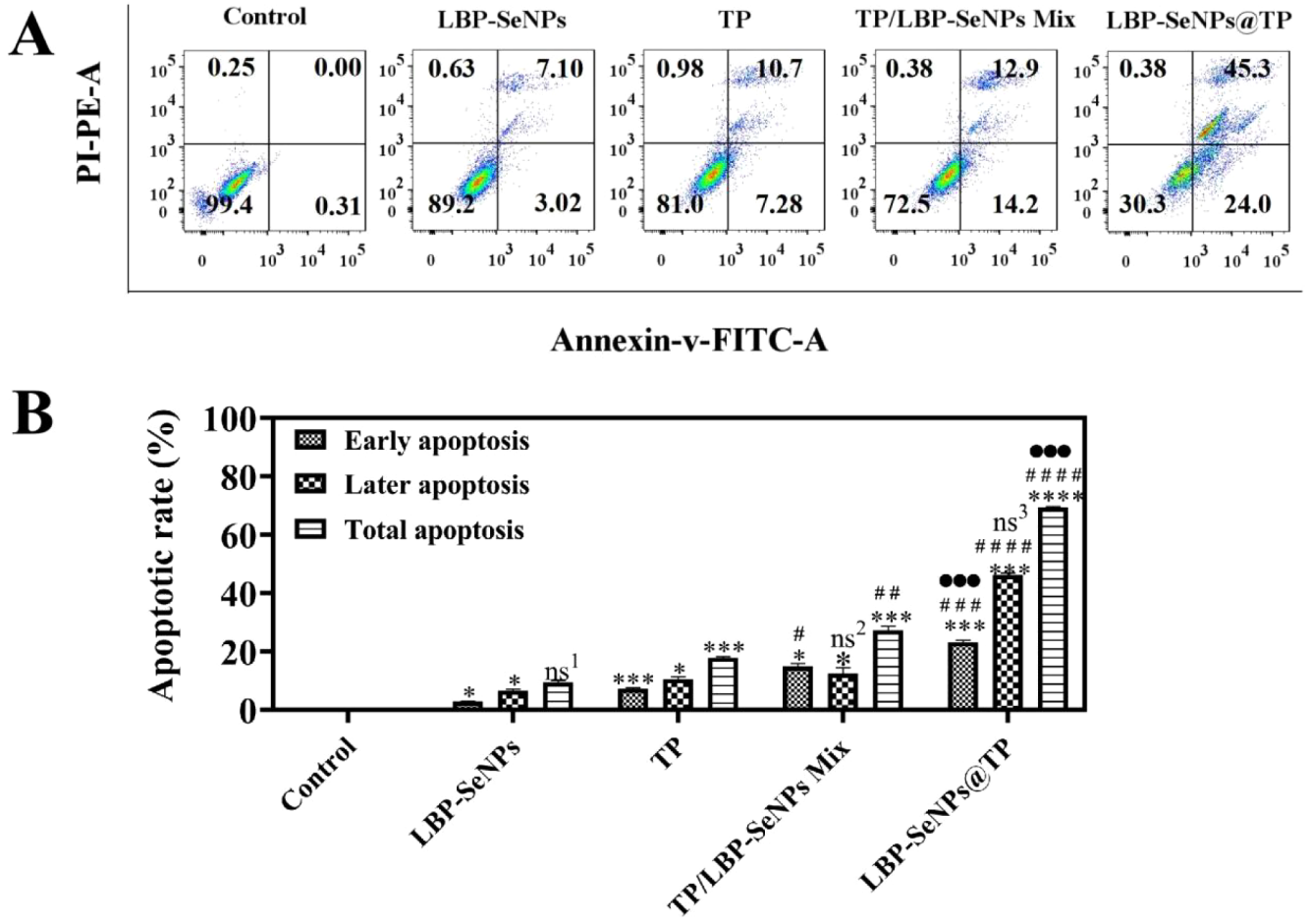

Figure 6. (A) Flow cytometry evaluation of Annexin V-FITC/PI staining apoptotic cells induced by LBP-SeNPs, TP, TP/LBP-SeNPs Mix, and LBP-SeNPs@TP. (B) Apoptotic rate (%) in LBP-SeNPs, TP, TP/LBP-SeNPs Mix, and LBP-SeNPs@TP. Versus the control group, $^{*}p < 0.05$, $^{***}p < 0.001$, $^{****}p < 0.0001$. Versus the TP group, $^{\#}p < 0.05$, $^{\#\#}p < 0.01$, $^{\#\#\#}p < 0.001$, $^{\#\#\#\#}p < 0.0001$. Versus the TP/LBP-SeNPs Mix group, $^{\bullet\bullet\bullet}p < 0.001$. Versus the control group, ns[1]. Versus the TP group, ns[2]. Versus the TP/LBP-SeNP Mix group, ns[3]. (mean ± SD, $n = 3$).

fluorescence for the LBP-SeNP group compared to the control group. However, the green-to-red fluorescence ratio increased to varying degrees for the TP ($p < 0.001$), TP/LBP-SeNPs Mix ($p < 0.001$), and LBP-SeNPs@TP ($p < 0.0001$) groups. Notably, the ratio was significantly higher in the LBP-SeNPs@TP group than those in TP ($p < 0.0001$) and TP/LBP-SeNPs Mix ($p < 0.0001$) groups. No significant difference was observed between the TP and TP/LBP-SeNPs Mix groups. These results were possibly attributed to the sustained release of LBP-SeNPs@TP, allowing for greater accumulation of TP within the mitochondria, thus leading to a more pronounced decrease in MMP.

3.7. LBP-SeNPs@TP-Induced Intracellular ROS Generation. Mitochondria serve as critical sites for intracellular ROS production. Excessive ROS production can trigger mitochondrial dysfunction, ultimately leading to cell apoptosis.[17] Therefore, we detected whether LBP-SeNPs@TP promoted the overproduction of intracellular ROS in Pan02 cells. DCFH-DA fluorescence assay was used to analyze the ROS levels in Pan02 cells treated with LBP-SeNPs, TP, TP/LBP-SeNPs Mix, and LBP-SeNPs@TP for 48 h. The detection principle is that once DCFH-DA enters the cell, it is hydrolyzed by intracellular esterases into DCFH (dichlorodihydrofluorescein). ROS within cells can oxidize nonfluorescent DCFH to generate fluorescent DCF (dichlorofluorescein). The fluorescence intensity is proportional to the level of ROS, and the intracellular ROS level can be measured by detecting the fluorescence intensity of DCF. Compared with the control group, the fluorescence intensity of the LBP-SeNPs group remained statistically similar (Figure 8). However, a gradual increase in fluorescence intensity was observed in the TP ($p < 0.01$), TP/LBP-SeNPs Mix ($p < 0.001$), and LBP-SeNPs@TP ($p < 0.0001$) groups. There was no significant difference between the TP and TP/LBP-SeNPs Mix groups, indicating that ROS overproduction was mainly triggered by TP. The ROS level was significantly elevated in the LBP-SeNPs@TP group compared to the TP ($p < 0.0001$) and TP/LBP-SeNPs Mix ($p < 0.0001$) groups. The results demonstrated that TP triggered ROS overproduction and LBP-SeNPs enhanced the ROS levels of TP, likely through the sustained release of TP from LBP-SeNPs@TP. The results of ROS production, MMP change, and apoptosis levels were basically consistent, indicating that LBP-SeNPs@TP could increase ROS levels, decrease MMP and enhance apoptosis in Pan02 cells.

3.8. LBP-SeNPs@TP-Induced Apoptosis-Related mRNA Expression Analysis. Our previous study[28] demonstrated that TP promoted apoptosis of Pan02 cells by regulating the expression of Bax, Bcl-2, Cyt C, and Caspase-3. We verified the expression changes of relevant mRNA

https://doi.org/10.1021/acsomega.4c04743
ACS Omega 2025, 10, 17108−17122

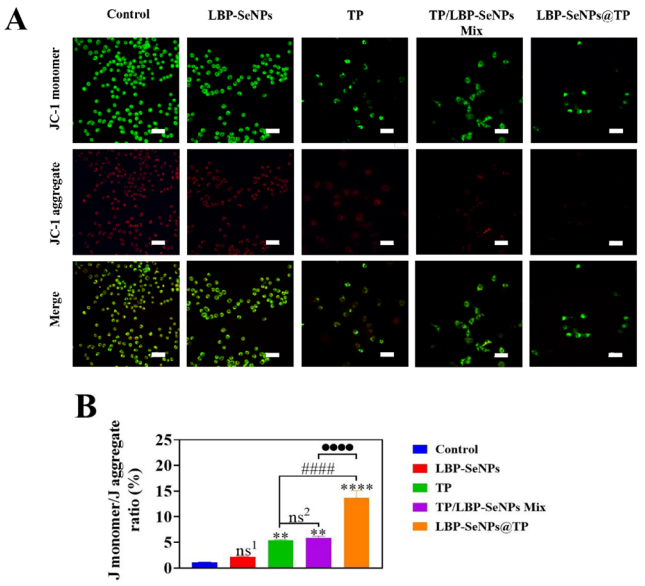

Figure 7. Effect of each group on the mitochondrial membrane potential of Pan02 cells detected by the JC-1 staining method. (A) Fluorescence microscope images of Pan02 cells treated with JC-1. (scale, 50 μm). (B) Quantitative analysis of J monomer/J aggregate ratio (%) after drug treatment in Pan02 cells. Versus the control group, $^{**}p < 0.01$, $^{****}p < 0.0001$. Versus the TP group, $^{\#\#\#\#}p < 0.0001$. Versus the TP/LBP-SeNPs Mix group, $^{\bullet\bullet\bullet\bullet}p < 0.0001$. Versus the control group, ns^1. Versus TP group, ns^2. (mean ± SD, n = 3).

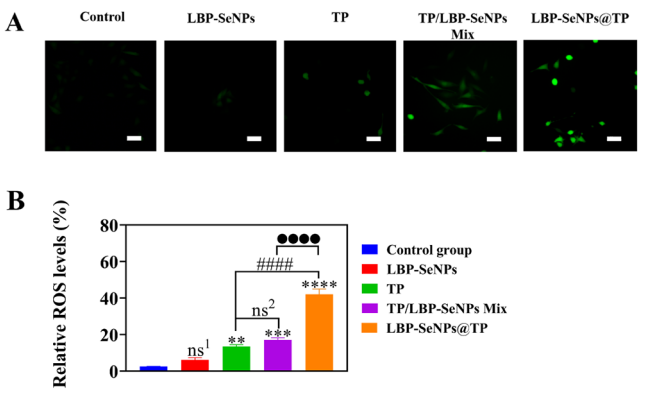

Figure 8. (A) Changes of intracellular ROS generation induced by LBP-SeNPs, TP, TP/LBP-SeNPs Mix, and LBP-SeNPs@TP in Pan02 cells (scale bar, 50 μm). (B) Quantitative analysis of relative ROS levels (%) induced by LBP-SeNPs, TP, TP/LBP-SeNPs Mix, and LBP-SeNPs@TP in Pan02 cells. Versus the control group, $^{**}p < 0.01$, $^{***}p < 0.001$, $^{****}p < 0.0001$. Versus the TP group, $^{\#\#\#\#}p < 0.0001$. Versus the TP/LBP-SeNPs Mix group, $^{\bullet\bullet\bullet\bullet}p < 0.0001$. Versus the control group, ns^1. Versus the TP group, ns^2. (mean ± SD, n = 3).

through the RT-qPCR assay. As shown in Figure 9, in comparison to the control group, the mRNA expression levels in the LBP-SeNPs group showed no significant change, while the mRNA expression levels of Bax, Cyt C, and Caspase-3 obviously increased, and the mRNA levels of Bcl-2 obviously decreased in the TP, TP/LBP-SeNPs Mix, and LBP-SeNPs@TP groups. The overall regulatory trend was as follows: LBP-SeNPs@TP > TP/LBP-SeNPs Mix > TP. The results demonstrated that LBP-SeNPs@TP induced the apoptosis of Pan02 cells by suppressing the expression of Bcl-2, enhancing Bax expression, promoting the release of Cyt C, and activating Caspase-3.

3.9. *In Vivo* Toxicity Assessment of LBP-SeNPs@TP.

Body weight was one of the indicators reflecting the toxicity of drugs in mice. As depicted in Figure 10, compared with the model group, the LBP-SeNPs group exhibited no significant difference in body weight within 14 days, indicating that the carrier had minimal impact on body weight and low toxicity. The body weight of the TP group showed maximum weight loss, while the other groups presented varying degrees of weight reduction. This indicated that the integration and encapsulation of TP with LBP-SeNPs effectively mitigated the toxicity of TP. There was no significant difference between the TP and TP/LBP-SeNPs Mix groups in the final body weight. Compared to the TP group, the final body weight obviously increased in the LBP-SeNPs@TP (low) ($p < 0.01$) and LBP-SeNPs@TP (high) ($p < 0.001$) groups. These results demonstrated that the toxicity was reduced in the LBP-SeNPs@TP group, which is possibly due to the sustained release and pH-responsive release, resulting in a more sustained and balanced concentration of TP *in vivo*.

The liver and kidney functions of mice were assessed using the corresponding kits. Liver function indicators, aspartate transaminase (AST) and alanine transaminase (ALT), and renal function indicators, creatinine (CRE) and blood urea nitrogen (BUN), were measured. As shown in Figure 11, there was no obvious difference between the model group and the LBP-SeNPs group, indicating that the carrier had no adverse effects on the liver and kidney. The AST, ALT, CRE, and BUN levels in the TP and TP/LBP-SeNPs Mix groups significantly increased, indicating hepatic and renal damage. For the TP/LBP-SeNPs Mix group, there was no significant difference in AST, ALT, CRE, and BUN levels compared with the free TP group, implying that physical mixing could not reduce the toxicity of TP. Compared with the model group, there was no significant change in the LBP-SeNPs@TP group, which indicated that LBP-SeNPs@TP may relieve the TP-induced toxicity in the liver and kidney.

TP mainly exerted toxic side effects on vital organs such as the heart, liver, kidneys, and testicular tissues. Therefore, histological examination using HE staining was conducted on the heart, liver, kidneys, and testicles of each group of mice. Figure 12 revealed that in the cardiac tissue, the myocardial fibers of the model and LBP-SeNPs groups were neatly arranged with distinct horizontal lines. Compared with the model group, the TP and the TP/LBP-SeNPs Mix groups exhibited a disordered arrangement of myocardial fibers and blurred horizontal lines. In the LBP-SeNPs@TP group, the damage was significantly improved compared with the TP group, with an orderly arrangement of myocardial fibers and clear transverse stripes. Examining the liver tissue, the hepatic cords of the model group and LBP-SeNPs group appeared orderly arranged with a clear lobule structure and slight edema. Compared with the model group, severe cellular edema and lytic necrosis occurred in the TP and TP/LBP-SeNPs Mix groups, while the LBP-SeNPs@TP group showed significant improvement in cell lytic necrosis. In renal tissue, the glomerular structures of the model and LBP-SeNPs groups were clear and intact. However, the TP and TP/LBP-SeNPs Mix groups showed glomerular atrophy and increased interstitial fibers. The glomerular atrophy in the LBP-SeNPs@TP group was significantly improved, with the morphology closely resembling the normal state. In the

https://doi.org/10.1021/acsomega.4c04743
ACS Omega 2025, 10, 17108−17122

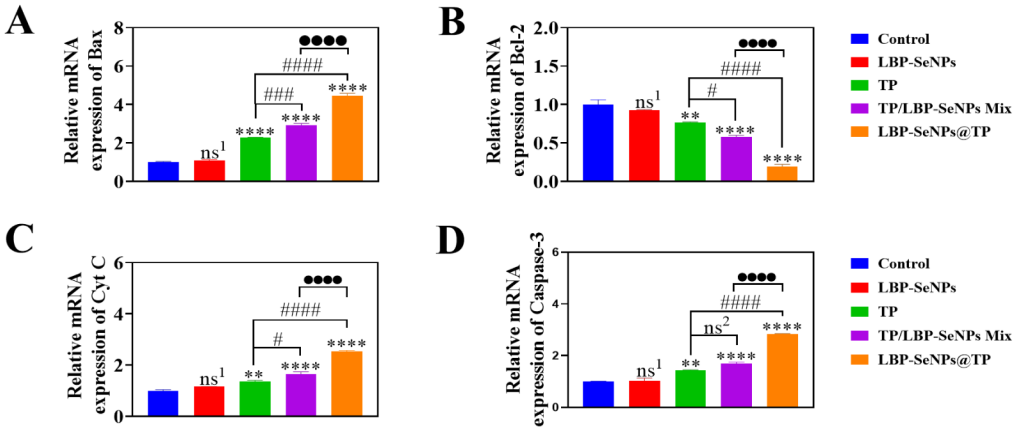

Figure 9. Effects of each group on the mRNA expression of (A) Bax, (B) Bcl-2, (C) Cyt C, and (D) Caspase-3 in Pan02 cells. Versus the control group,$^{**}p < 0.01$, $^{****}p < 0.0001$. Versus the TP group, $^{\#}p < 0.05$, $^{\#\#\#\#}p < 0.0001$. Versus the TP/LBP-SeNPs Mix group, $^{\bullet\bullet\bullet\bullet}p < 0.0001$. Versus the control group, ns^1. Versus the TP group, ns^2. (mean ± SD, $n = 3$).

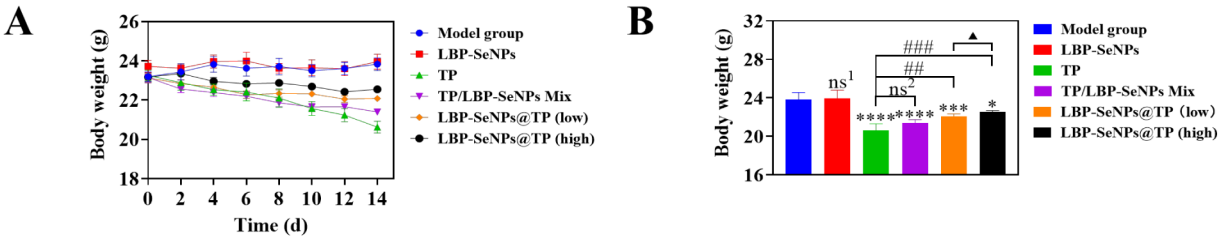

Figure 10. (A) Mouse body weight change curves in each group. (B) Body weight of mice in each group at the end of the experiment. Versus the model group, $^{*}p < 0.05$, $^{***}p < 0.001$, $^{****}p < 0.0001$. Versus the TP group, $^{\#\#}p < 0.01$, $^{\#\#\#}p < 0.001$. Versus the LBP-SeNPs@TP (low) group, $^{\blacktriangle}p < 0.05$. Versus the model group, ns^1. Versus the TP group, ns^2. (mean ± SD, $n = 5$).

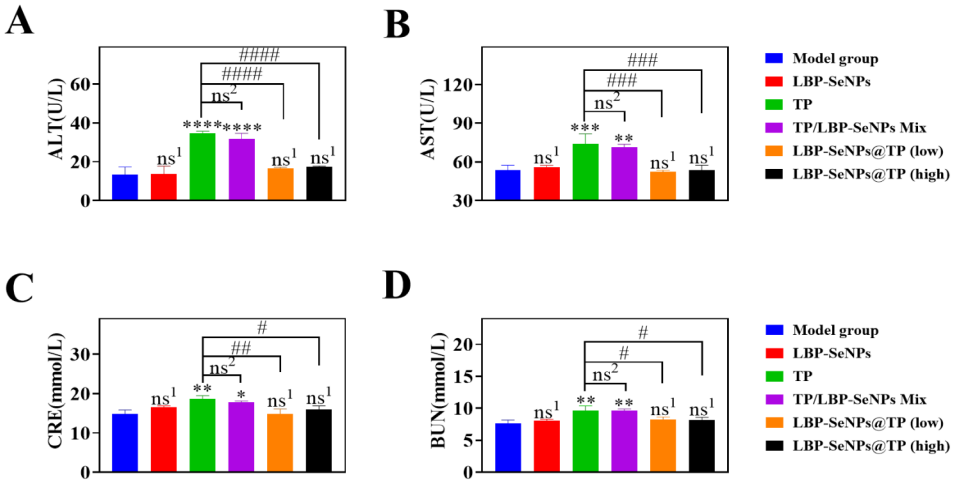

Figure 11. Biochemical parameters, (A) ALT, (B) AST, (C) CRE, and (D) BUN of each group. Versus the model group, $^{*}p < 0.05$, $^{**}p < 0.01$, $^{***}p < 0.001$, $^{****}p < 0.0001$. Versus the TP group, $^{\#}p < 0.05$, $^{\#\#}p < 0.01$, $^{\#\#\#}p < 0.001$, $^{\#\#\#\#}p < 0.0001$. Versus the model group, ns^1. Versus the TP group, ns^2. (mean ± SD, $n = 3$).

testicular tissues of the model group and LBP-SeNPs group, the testicular cells had normal morphology, well-developed structures, regular arrangement, and the presence of numerous mature sperm in the lumen. By contrast, the TP and TP/LBP-SeNPs Mix groups displayed a significant decrease in the number of mature sperm, disordered basal layer cells, and vacuolar degeneration in some cells. Interestingly, the morphology in the LBP-SeNPs@TP group was similar to that of the model group, with only minor disorders in the arrangement of basal layer cells. The above results indicated that LBP-SeNPs@TP caused minimal pathological damage and could reduce the toxicity of TP in the heart, liver, kidneys, and testes of mice.

3.10. *In Vivo* Antitumor Efficacy of LBP-SeNPs@TP.

The therapeutic effect of LBP-SeNPs@TP *in vivo* was a key indicator of its future medical potential. Tumor volume and weight were utilized as indicators to evaluate the *in vivo* antiproliferation effect of LBP-SeNPs@TP. Figure 13A showed the photographs of tumors in mice after 14 days, and the order of tumor volume was as follows: model group > LBP-SeNPs

https://doi.org/10.1021/acsomega.4c04743
ACS Omega 2025, 10, 17108−17122

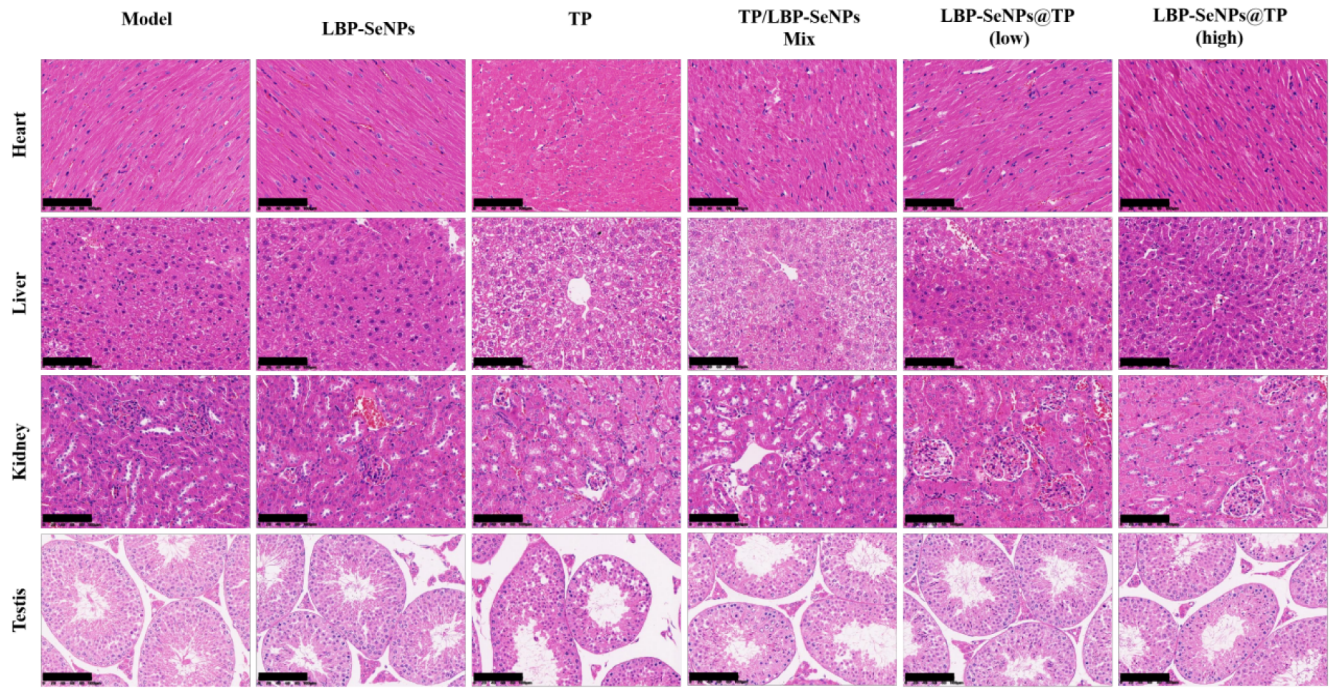

Figure 12. Histological staining of the heart, liver, kidney, and testis of mice in each group (scale bar, 50 μm).

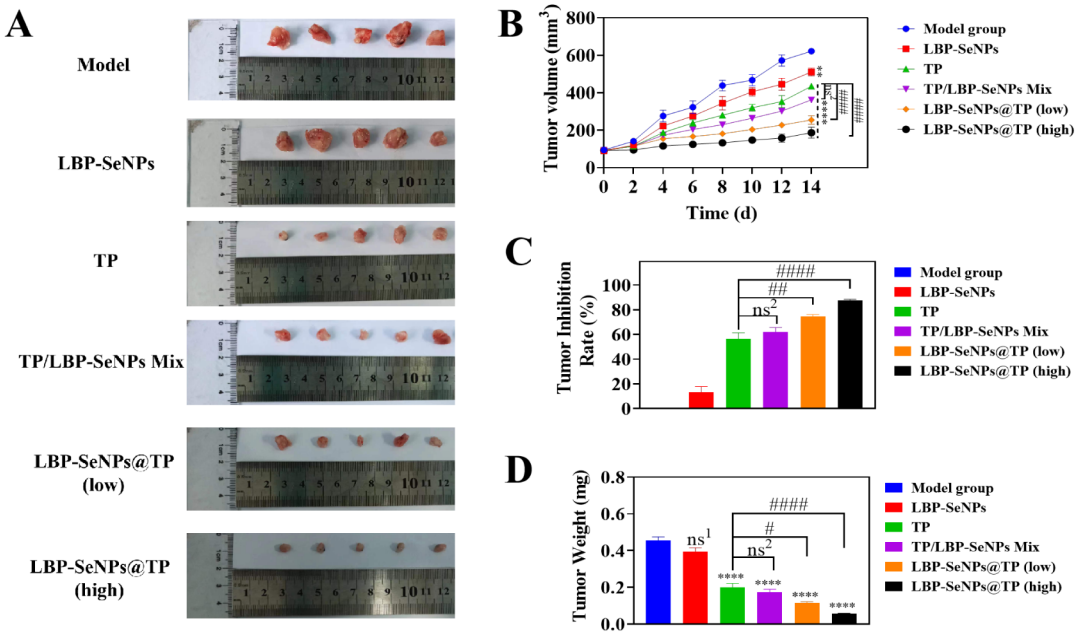

Figure 13. Evaluation of the antitumor effect. (A) Photographs of tumor in each group after 14 days of administration. (B) Changes in tumor volume of mice within 14 days of administration. (C) Tumor inhibition rate after 14 days of administration. Tumor inhibition rate (TIR) = [(tumor volume of the control group − tumor volume of drug group)/tumor volume of the control group] × 100%. (D) Tumor weight after 14 days of administration. Versus the model group, $^{**}p < 0.01$, $^{***}p < 0.001$. Versus the TP group, $^{\#}p < 0.05$, $^{\#\#}p < 0.01$, $^{\#\#\#\#}p < 0.0001$. Versus the model group, ns[1]. Versus the TP group, ns[2]. (mean ± SD, $n = 5$).

group > TP group > TP/LBP-SeNPs Mix group > LBP-SeNPs@TP (low) group > LBP-SeNPs@TP (high) group, as shown in Figure 13 A,B. Regarding tumor growth inhibition rate, a significant difference was observed between the TP and LBP-SeNPs@TP groups ($p < 0.01$, $p < 0.0001$), whereas no significant difference was noted between the TP and TP/LBP-SeNPs Mix groups (Figure 13C). The results of tumor weight were in alignment with the tumor inhibition rate, indicating that the therapeutic effect of LBP-SeNPs@TP was optimal.

3.11. Pathological Observation and Ki67 Analysis of Tumor Tissue. The antitumor activity was further evaluated through pathological morphology observation and Ki67 analysis of tumor tissue. The HE staining results in Figure 14 showed that the tumor cells in the model group and LBP-SeNPs group exhibited a dense distribution, enlarged nuclei with irregular arrangement, and no signs of apoptosis. In contrast, the TP, TP/LBP-SeNPs Mix, and LBP-SeNPs@TP groups showed varying degrees of inhibitory effects. The TP

https://doi.org/10.1021/acsomega.4c04743
ACS Omega 2025, 10, 17108−17122

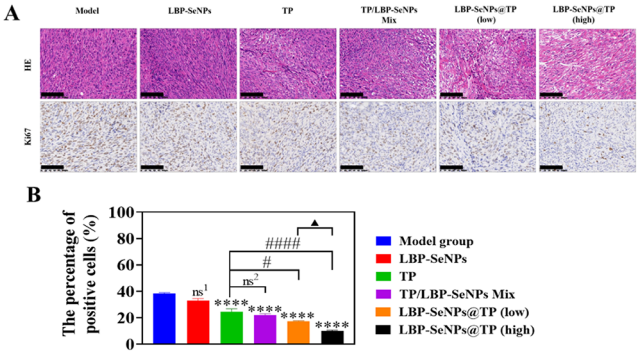

Figure 14. (A) Histological and Ki67 staining of tumor in each group (scale, 50 μm). (B) The percentage of Ki67-positive cells in pancreatic cancer tissue. Versus the model group, ****$p < 0.0001$. Versus the TP group, $^{\#}p < 0.05$, $^{\#\#\#\#}p < 0.0001$. Versus the LBP-SeNPs@TP (low) group, $^{\blacktriangle}p < 0.05$. Versus the model group, ns^1. Versus the TP group, ns^2. (mean ± SD, $n = 5$).

and TP/LBP-SeNPs Mix groups showed a marked decrease in tumor cells, along with disordered cell arrangement and nuclear pyknosis or disappearance. Furthermore, the LBP-SeNPs@TP group exhibited severe damage to cell structures, evident apoptosis, and the formation of cell cavities. Ki67 staining, a commonly utilized method for evaluating tumor proliferation, indicated brownish-yellow positive expression in cancer cells. As shown in Figure 14, there was significant expression of Ki67 in the model group and LBP-SeNPs group, while the expression in the TP group ($p < 0.0001$), TP/LBP-SeNPs Mix group ($p < 0.0001$), LBP-SeNPs@TP (low) group ($p < 0.0001$), and LBP-SeNPs@TP group (high) ($p < 0.0001$) was significantly reduced. Compared to the TP group, the change in antigen expression in the TP/LBP-SeNPs Mix group was not prominent. However, LBP-SeNPs@TP (low) ($p < 0.05$) and LBP-SeNPs@TP (high) ($p < 0.0001$) significantly enhanced the percentage of positive cells, with the high-dose group exhibiting a superior inhibitory effect ($p < 0.05$). The results demonstrated that the effect of inducing apoptosis in pancreatic cancer cells in the LBP-SeNPs@TP group was the best at equivalent doses of TP.

3.12. Expression of Related Apoptotic Genes Regulated by LBP-SeNPs@TP in Tumor Tissue. It was found that TP could induce the apoptosis of pancreatic cancer cells by inhibiting the expression of Bcl-2, upregulating the expression of Bax, increasing the release of Cyt C, and activating Caspase-3. RT-qPCR analysis was used to verify the expression changes of related mRNA. As shown in Figure 15, compared with the model group, the four genes in the LBP-SeNPs group did not change significantly, while the other groups showed different degrees of decreased expression of Bcl-2 and increased expression of Bax, Cyt C, and Caspase-3. Among them, the mRNA expression changes in the LBP-SeNPs@TP groups were particularly significant compared to those in the TP group, with the best induction of apoptosis and a significant statistical difference. Furthermore, the high-dose group induced more apoptosis ($p < 0.01$, $p < 0.01$, $p < 0.001$, $p < 0.0001$). Additionally, the protein expression levels of Bax, Bcl-2, Cyt-C, Caspase-3, and Cleaved-Caspase-3 in tumor tissue were detected by immunohistochemistry. The results were basically consistent with those from RT-qPCR (Figure S4).

4. DISCUSSION

According to previous research,[5−7,28] triptolide has demonstrated significant antipancreatic cancer effects. However, its application has been hampered by drawbacks such as poor water solubility and high toxicity. Nanotechnology has been widely used for drug delivery, and selenium nanoparticles are favored due to their excellent water solubility, low toxicity, and suitable biocompatibility. However, the stability of SeNPs remains a challenge, necessitating modifications. Traditional Chinese medicine polysaccharides, with highly branched structures and rich −OH functional groups[20,29] facilitated the formation of Se−O bonds[18] and promoted the stable existence of SeNPs. Simultaneously, Chinese medicine polysaccharides have antioxidant activity, low toxicity, and natural compatibility with the human body, making them excellent candidates as carriers. In this study, four common Chinese medicine polysaccharides, *Ganoderma lucidum* polysaccharides, *Astragalus* polysaccharides, *Brown* algae polysaccharides, and *Lycium barbarum* polysaccharides, were selected as modifiers. Among them, LBP-modified SeNPs exhibited the best dispersivity, with a particle size of 66.32 ± 0.26 nm and a Zeta potential of 17.17 ± 1.77 mV. Furthermore, these nanoparticles maintained

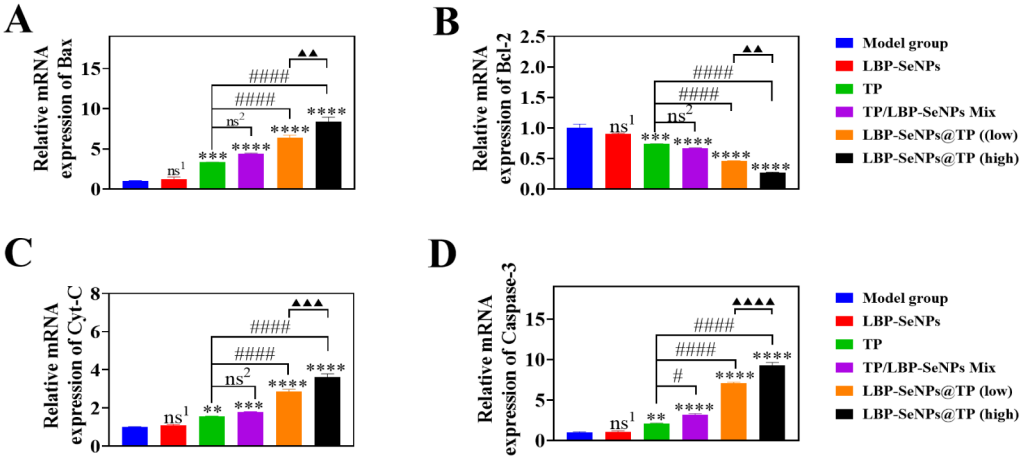

Figure 15. Expression changes of apoptosis-related mRNA, (A) Bax, (B) Bcl-2, (C) Cyt-C, and (D) Caspase-3, in tumor tissue. Versus the model group, **$p < 0.01$, ***$p < 0.001$, ****$p < 0.0001$. Versus the TP group, $^{\#}p < 0.05$, $^{\#\#\#\#}p < 0.0001$. Versus the LBP-SeNPs@TP (low) group, $^{\blacktriangle\blacktriangle}p < 0.05$, $^{\blacktriangle\blacktriangle\blacktriangle}p < 0.05$, $^{\blacktriangle\blacktriangle\blacktriangle\blacktriangle}p < 0.05$. Versus the model group, ns^1. Versus the TP group, ns^2. (mean ± SD, $n = 3$).

https://doi.org/10.1021/acsomega.4c04743
ACS Omega 2025, 10, 17108−17122

stability for 42 days without any obvious change in particle size.

Subsequently, TP was successfully loaded onto the carrier LBP-SeNPs through the formation of hydrogen bonds and physical adsorption.[18] Preliminary experimental results indicated that when the molar ratio of input Se:TP was $\leq$ 3:1, the resulting product exhibited poor water dispersivity. Therefore, molar ratios of input Se:TP at 5:1, 10:1, and 20:1 were used to examine the optimal proportion of LBP-SeNPs@TP. By evaluating the particle size, PDI, Zeta potential, encapsulation efficiency, and drug loading of LBP-SeNPs@TP, the optimal feeding molar ratio of LBP-SeNPs to TP was determined to be 5:1, yielding the smallest particle size and the highest drug loading. TP was successfully attached to LBP-SeNPs, which was confirmed by UV−vis, FT-IR, HPLC, and TEM, with uniform dispersion, regular spherical morphology, and a particle size of 113.8 $\pm$ 3.44 nm. As reported, nanoparticles with sizes between 60 and 200 nm are more likely to penetrate the blood vessel wall and enter tumor cells due to the abundance of blood vessels, the wide gaps between blood vessel walls, and the poor structural integrity in tumor tissue.[30] Therefore, the obtained nanodrug satisfied the necessary criteria. Stability experiments demonstrated that LBP-SeNPs@TP remained stable in aqueous solution for 35 days at 4 °C and in various biological media, including DMEM, FBS, PBS, and DMEM + 10% FBS at 37 °C for 24 h. *In vitro* release experiments showed that LBP-SeNPs@TP displayed sustained and acid-dependent release effects, facilitating drug accumulation in the acidic tumor microenvironment.

To investigate the toxicity of LBP-SeNPs@TP toward normal hepatocytes and pancreatic cancer cells, the cell viability test was conducted to investigate the IC_{50} values. LBP-SeNPs@TP significantly inhibited the proliferation of Pan02 cells and reduced its toxic effects on L02 cells. Subsequently, the apoptosis assay verified that LBP-SeNPs@TP had obviously enhanced inhibitory effect on the proliferation of pancreatic cancer cells. Mitochondrial-mediated cell apoptosis was identified as a crucial pathway of apoptosis. Under physiological conditions, the mitochondrial permeability transition pore (MPTP) maintains mitochondrial homeostasis by transiently releasing a limited amount of reactive oxygen species (ROS), which supports cell growth. However, under intense stimulation, such as drug exposure, the MPTP remains open in an irreversible way, leading to the release of excessive ROS. This triggers an oxidative stress reaction that compromises mitochondrial membrane integrity, releases proapoptotic proteins such as Cyt C, and activates caspase-3, ultimately culminating in apoptosis. Additionally, the expression of the antiapoptosis protein Bcl-2 was downregulated, while the expression of the apoptosis-promoting protein Bax was upregulated. This cascade results in increased ROS levels, decreased mitochondrial membrane potential (MMP), altered mitochondrial membrane permeability, and accelerated apoptosis.[31] To confirm whether LBP-SeNPs@TP induced the apoptosis of Pan02 cells via the mitochondrial apoptosis pathway, we assessed the effects of the drugs on MMP and ROS levels following 48 h of exposure. The results showed that MMP decreased and intracellular ROS increased significantly. Subsequently, RT-qPCR was used to detect the expression levels of apoptotic genes Bax, Bcl-2, Cyt C, and Caspase-3. The results showed that the mRNA expression of Bcl-2 decreased, while the mRNA expression of Bax, Cyt C, and Caspase-3 increased. The above results demonstrated that LBP-SeNPs@TP induced cell apoptosis by inhibiting the activation of Bcl-2, promoting the expression of Bax, triggering an increase in ROS production, reducing the MMP, altering the permeability of the mitochondrial membrane, releasing Cyt C, and facilitating the activation of Caspase-3. Compared to free TP and TP/LBP-SeNPs Mix, LBP-SeNPs@TP showed superior antitumor efficiency.

To investigate *in vivo* toxicity and antitumor efficiency of LBP-SeNPs@TP, Pan02 homologous mice were chosen to establish the mouse model of pancreatic cancer and were treated via tail vein injection for 14 days. By monitoring changes in body weight, analyzing histomorphology via HE staining, and assessing liver and kidney function indicators within the 14-day period, it was observed that the LBP-SeNPs group exhibited no significant difference compared to the model group. However, the TP group and TP/LBP-SeNPs Mix group showed significant organ damage. Notably, mice in the LBP-SeNPs@TP groups were not significantly damaged. These findings suggested that LBP-SeNPs@TP was capable of reducing the toxicity of TP in various organs of mice.

In vivo antitumor efficiency of LBP-SeNPs@TP on the Pan02 homologous mouse model was examined. Tumor volume and inhibition rate serve as direct indicators of a drug's ability to suppress tumor growth. Our findings revealed that the LBP-SeNPs@TP group exhibited significantly superior antitumor effects compared to equivalent doses of free TP and the TP/LBP-SeNPs Mix group. The HE staining of tumor tissue sections provided clear insights into the pathological and histological changes of tumors in each treatment group. Notably, the LBP-SeNPs@TP groups displayed a marked reduction in tumor cells and severe damage to the tumor structure. Ki67 antigen staining, a reliable marker for evaluating tumor proliferation, further supported our observations. The histochemical analysis of Ki67 expression revealed a notable decrease in the the LBP-SeNPs@TP groups compared to the free TP and TP/LBP-SeNPs Mix groups, indicating a superior inhibitory effect on tumor proliferation. To gain a deeper understanding of the molecular mechanisms involved, we conducted RT-qPCR assays to assess the expression levels of apoptotic genes Bax, Bcl-2, Cyt C, and Caspase-3 in each treatment group. The results confirmed that LBP-SeNPs@TP effectively suppressed the proliferation of pancreatic cancer cells by inducing apoptosis through the mitochondrial pathway *in vivo*. Additionally, the protein expression levels of Bax, Bcl-2, Cyt C, Caspase-3, and Cleaved-Caspase-3 in tumor tissue were detected by immunohistochemistry. The results were basically consistent with those obtained by RT-qPCR (Figure S4). These findings align with our previous *in vitro* results, further validating the antitumor potential of LBP-SeNPs@TP.

5. CONCLUSIONS

In summary, LBP-SeNPs were successfully synthesized as effective carriers to encapsulate TP, thereby preparing the nanodrug LBP-SeNPs@TP. Both *in vivo* and *in vitro* studies demonstrated that this nanodrug exhibited enhanced anti-pancreatic cancer efficacy while significantly reducing toxicity. Further research revealed that the antitumor mechanism of LBP-SeNPs@TP involved inducing cancer cell apoptosis. This was achieved by inhibiting the expression of Bcl-2, promoting the upregulation of Bax, increasing the release of Cyt C, and activating Caspase-3. Collectively, our findings suggest that LBP-SeNPs serve as excellent carriers for poorly soluble drugs,

https://doi.org/10.1021/acsomega.4c04743
ACS Omega 2025, 10, 17108−17122

and LBP-SeNPs@TP holds promise as a potential candidate for the treatment of pancreatic cancer.

■ ASSOCIATED CONTENT

Supporting Information

The Supporting Information is available free of charge at https://pubs.acs.org/doi/10.1021/acsomega.4c04743.

Photographs of SeNP aqueous solution without any modification; standard curve of TP detected by UV−vis spectra; standard curve of TP detected by HPLC spectra; immunohistochemical (IHC) analyze: method and results (PDF)

■ AUTHOR INFORMATION

Corresponding Authors

Zhenqiang Zhang − *Academy of Chinese Medicine Sciences, Henan University of Chinese Medicine, Zhengzhou 450046, PR China*; Email: zhang_zhenqiang@126.com

Xuebin Zhao − *Technology Center, China Tobacco Henan Industrial Co., Ltd., Zhengzhou 450000, PR China*; orcid.org/0009-0007-1004-775X; Email: zhaoxuebin116@163.com

Huahui Zeng − *Academy of Chinese Medicine Sciences, Henan University of Chinese Medicine, Zhengzhou 450046, PR China*; Email: hhzeng@hactcm.edu.cn

Authors

Xiaofang Li − *Academy of Chinese Medicine Sciences, Henan University of Chinese Medicine, Zhengzhou 450046, PR China; The First Affiliated Hospital of Henan University of Chinese Medicine, Zhengzhou 450099, PR China*; orcid.org/0000-0002-3150-9198

Yunfang Su − *Academy of Chinese Medicine Sciences, Henan University of Chinese Medicine, Zhengzhou 450046, PR China; The First Affiliated Hospital of Henan University of Chinese Medicine, Zhengzhou 450099, PR China*

Na Lin − *Rehabilitation Department, Kaifeng Hospital of Traditional Chinese Medicine, Kaifeng 475000, PR China*

Yujie Chen − *Academy of Chinese Medicine Sciences, Henan University of Chinese Medicine, Zhengzhou 450046, PR China*

Zhonghua Li − *Academy of Chinese Medicine Sciences, Henan University of Chinese Medicine, Zhengzhou 450046, PR China*; orcid.org/0000-0003-0458-3664

Complete contact information is available at: https://pubs.acs.org/10.1021/acsomega.4c04743

Notes

The authors declare no competing financial interest.

Ethics Approval and Consent to Participate: All animals were raised in the Laboratory Animal Building of the Experimental Animal Center of Henan University of Chinese Medicine, which is equipped with feeding and experimental conditions for experimental animals and meets the requirements for standardized animal experiments. The animal experiment work was approved by the Experimental Animal Ethics Committee of Henan University of Traditional Chinese Medicine (No. DWLL202110005).

■ ACKNOWLEDGMENTS

This work was supported by the National Natural Science Foundation of China (82104400, 82274612), the National Key Research and Development Project (2022YFC3502100), the Postdoctoral Research Project of Henan Province (HN2022084), the Scientific and Technological Brainstorm Project of Henan Province under Grant (212102311086, 232102311223), the Joint Research Fund of the Science and Technology R&D Plan of Henan Province (222301420068), and the Science and Technology Project of China Tobacco Henan Industrial Co., Ltd. (AW2023005).

■ REFERENCES

(1) Khan, S.; Chauhan, N.; Yallapu, M. M.; Ebeling, M. C.; Balakrishna, S.; Ellis, R. T.; Thompson, P. A.; Balabathula, P.; Behrman, S. W.; Zafar, N.; Singh, M. M.; Halaweish, F. T.; Jaggi, M.; Chauhan, S. C. Nanoparticle formulation of ormeloxifene for pancreatic cancer. *Biomaterials* **2015**, *53*, 731−743.

(2) Ryan, D. P.; Hong, T. S.; Bardeesy, N. Pancreatic adenocarcinoma. *N. Engl. J. Med.* **2014**, *371*, 1039−1049.

(3) Vincent, A.; Herman, J.; Schulick, R.; Hruban, R. H.; Goggins, M. Pancreatic cancer. *Lancet* **2011**, *378*, 607−620.

(4) Tong, L.; Zhao, Q. F.; Datan, E.; Lin, G. Q.; Minn, I.; Pomper, M. G.; Yu, B.; Romo, D.; He, Q. L.; Liu, J. O. Triptolide: reflflections on two decades of research and prospects for the future. *Nat. Prod. Rep.* **2021**, *38* (4), 843−860.

(5) Noel, P.; Hoff, D. D. V.; Saluja, A. K.; Velagapudi, M.; Borazanci, E.; Han, H. Triptolide and Its Derivatives as Cancer Therapies. *Trends Pharmacol. Sci.* **2019**, *40* (5), 327−341.

(6) Zhang, C.; He, X.- J.; Li, L.; Lu, C.; Lu, A.- P. Effect of the Natural Product Triptolide on Pancreatic Cancer: A Systematic Review of Preclinical Studies. *Front. Pharmacol.* **2017**, *8*, 490.

(7) Li, M. Y.; Tang, D. D.; Yang, T.; Qian, D.; Xu, R. C. Apoptosis Triggering, an Important Way for Natural Products From Herbal Medicines to Treat Pancreatic Cancers. *Front. Pharmacol.* **2022**, *12*, 796300.

(8) Li, X.; Mao, Y. L.; Li, K.; Shi, T. Y.; Yao, H. M.; Yao, J. H.; Wang, S. J. Pharmacokinetics and tissue distribution study in mice of triptolide-loaded lipid emulsion and accumulation effect on pancreas. *Drug Delivery.* **2016**, *23*, 1344−1354.

(9) Lin, C.; Zhang, X.; Chen, H.; Bian, Z.; Zhang, G.; Riaz, M.K.; Tyagi, D.; Lin, G.; Zhang, Y.; Wang, J.; et al. Dual-ligand modified liposomes provide effective local targeted delivery of lung-cancer drug by antibody and tumor lineage-homing cell-penetrating peptide. *Drug Delivery* **2018**, *25*, 256−266.

(10) Zheng, W.; Wang, C.; Ding, R. H.; Huang, Y. H.; Li, Y. Y.; Lu, Y. Triptolide-loaded nanoparticles targeting breast cancer *in vivo* with reduced toxicity. *Int. J. Pharm.* **2019**, *572*, 118721.

(11) Ling, D. S.; Xia, H. P.; Park, W.; Hackett, M. J.; Song, C. Y.; Na, K.; Hui, K. M.; Hyeon, T. pH-sensitive nanoformulated triptolide as a targeted therapeutic strategy for hepatocellular carcinoma. *ACS Nano* **2014**, *8*, 8027−8039.

(12) Wang, C.; Liu, B.; Xu, X. L.; Zhuang, B.; Li, H. X.; Yin, J. Q.; Cong, M. Y.; Xu, W.; Lu, A. P. Toward targeted therapy in chemotherapy-resistant pancreatic cancer with a smart triptolide nanomedicine. *Oncotarget* **2016**, *7*, 8360.

(13) Yang, M.; Gu, Y.; Yang, D.; Tang, X.; Liu, J. Development of triptolide-nanoemulsion gels for percutaneous administration: physicochemical, transport, pharmacokinetic and pharmacodynamic characteristics. *J. Nanobiotechnol.* **2017**, *15* (1), 88.

(14) Liu, H.- J.; Wang, M.; Hu, X.; Shi, S.; Xu, P. Enhanced Photothermal Therapy through the In Situ Activation of a Temperature and Redox Dual-Sensitive Nanoreservoir of Triptolide. *Small* **2020**, *16* (38), 2003398.

(15) Liu, H. B.; Zhang, H.; Yin, N.; Zhang, Y.; Gou, J. X.; Yin, T.; He, H. B.; Ding, H.; Zhang, Y.; Tang, X. Sialic acid-modified dexamethasone lipid calcium phosphate gel core nanoparticles for target treatment of kidney injury. *Biomater. Sci.* **2020**, *8*, 3871−3884.

(16) Luo, L. Y.; He, H. Y.; Li, C. H.; He, Y. Q.; Hao, Z. N.; Wang, S.; Zhao, Q. Q.; Liu, Z. W.; Gao, D. W. Near-Infrared Responsive

Bimetallic Nanovesicles for Enhanced Synergistic Chemophotothermal Therapy. *ACS Biomater. Sci. Eng.* **2019**, *5* (3), 1321−1331.
(17) Xia, Y.; Xiao, M.; Zhao, M.; Xu, T.; Guo, M.; Wang, C.; Li, Y.; Zhu, B.; Liu, H. Doxorubicin-loaded functionalized selenium nanoparticles for enhanced antitumor effiffifficacy in cervical carcinoma therapy. *Mater. Sci. Eng.* **2020**, *106*, 110100.
(18) Liu, W.; Li, X. L.; Wong, Y. S.; Zheng, W. J.; Zhang, Y. B.; Cao, W. Q.; Chen, T. F. Selenium nanoparticles as a carrier of 5-fluorouracil to achieve anticancer synergism. *ACS Nano* **2012**, *6* (8), 6578−6591.
(19) Tang, S.; Wang, T.; Jiang, M. Y.; Huang, C. X.; Lai, C. H.; Fan, Y. M.; Yong, Q. Construction of arabinogalactans/selenium nanoparticles composites for enhancement of the antitumor activity. *Int. J. Biol. Macromol.* **2019**, *128*, 444−451.
(20) Zhang, F.; Zhang, X.; Guo, S.; Cao, F. N.; Zhang, X. F.; Wang, Y. Q. J. Z.; Liu, J. Z.; Qian, B. W.; Yan, Y. C.; Chen, P. D.; Xu, C. L.; Liu, C. M.; Qian, D. W.; Duan, J. A. An acidic heteropolysaccharide from Lycii fructus: Purification, characterization, neurotrophic and neuroprotective activities *in vitro*. *Carbohyd. Polym.* **2020**, *249*, 116894.
(21) Liu, H. J.; Qin, Y.; Zhao, Z. H.; Zhang, Y.; Yang, J. H.; Zhai, D. H.; Cui, F.; Luo, C.; Lu, M. X.; Liu, P. P.; Xu, H. W.; Li, K.; Sun, B.; Chen, S.; Zhou, H. G.; Yang, C.; Sun, T. Lentinan-functionalized Selenium nanoparticles target tumor cell mitochondria *via* TLR4/TRAF3/MFN1 pathway. *Theranostics* **2022**, *12* (17), 7645.
(22) Wang, L.; Li, C.; Huang, Q.; Fu, X. Biofunctionalization of selenium nanoparticle with a polysaccharide from Rosa roxburghii fruit and its protective effect against H_2O_2-induced apoptosis in INS-1 cells. *Food Funct.* **2019**, *10*, 539−553.
(23) Gao, X.; Li, X.; Mu, J.; Ho, C. T.; Su, J.; Zhang, Y.; Lin, X.; Chen, Z.; Li, B.; Xie, Y. Preparation, physicochemical characterization, and anti-proliferation of selenium nanoparticles stabilized by Polyporus umbellatus polysaccharide. *Int. J. Biol. Macromol.* **2020**, *152* (1), 605−615.
(24) Huo, X. L.; Zhang, Y. Q.; Jin, X. C.; Li, Y. A.; Zhang, L. A novel synthesis of selenium nanoparticles encapsulated PLGA nanospheres with curcumin molecules for the inhibition of amyloid β aggregation in Alzheimer's disease. *J. Photochem. Photobiol., B* **2019**, *190*, 98−102.
(25) Patil, S.; Lis, L. G.; Schumacher, R. J.; Norris, B. J.; Morgan, M. L.; Cuellar, R. A. D.; Blazar, B. R.; Suryanarayanan, R.; Gurvich, V. J.; Georg, G. I. Phosphonooxymethyl Prodrug of Triptolide: Synthesis, Physicochemical Characterization, and Efficacy in Human Colon Adenocarcinoma and Ovarian Cancer Xenografts. *J. Med. Chem.* **2015**, *58*, 9334−9344.
(26) Liu, G. Y.; Yang, X.; Zhang, J. X.; Liang, L.; Miao, F.; Ji, T.; Ye, Z. Q.; Chu, M.; Ren, J. Y.; Xu, X. Synthesis, stability and anti-fatigue activity of selenium nanoparticles stabilized by Lycium barbarum polysaccharides. *Int. J. Of Biol. Macromol.* **2021**, *179*, 418−428.
(27) Huang, Y.; He, L.; Liu, W.; Fan, C.; Zheng, W.; Wong, Y.- S.; Chen, T. Selective cellular uptake and induction of apoptosis of cancer-targeted selenium nanoparticles. *Biomaterials* **2013**, *34*, 7106−7116.
(28) Tan, X. K.; Zhu, X.; Xu, D. J.; Shi, Y. M.; Wang, Z. Z.; Cao, M. Z.; Hu, K.; Zhao, L. Z.; Zhao, J. W.; Miao, M. S.; Zeng, H. H.; Wu, X. X. A mitochondria-targeted nano-platform for pancreatic cancer therapy. *Front. Chem.* **2022**, *10*, 951434.
(29) Zhang, J. X.; Yang, X.; Ji, T.; Wen, C. T.; Ye, Z. Q.; Liu, X. F.; Liang, L.; Liu, G. Y.; Xu, X. Digestion and absorption properties of Lycium barbarum polysaccharides stabilized selenium nanoparticles. *Food Chem.* **2022**, *373*, 131637.
(30) Matsumura, Y.; Maeda, H. A new concept for macromolecular therapeutics in cancer chemotherapy: Mechanism of tumoritropic accumulation of proteins and the antitumor agent smancs. *Cancer Res.* **1986**, *46* (12), 6387−6392.
(31) Zhang, R. F.; Humphreys, I.; Sahu, R. P.; Shi, Y.; Srivastava, S. K. *In vitro* and *in vivo* induction of apoptosis by capsaicin in pancreatic cancer cells is mediated through ROS generation and mitochondrial death pathway. *Apoptosis* **2008**, *13*, 1465−1478.

https://doi.org/10.1021/acsomega.4c04743
ACS Omega 2025, 10, 17108−17122